THE JOURNAL OF PHYSICAL CHEMISTRY B

Article

pubs.acs.org/JPCB

# Density Functional Study for Homodendrimers and Amphiphilic Dendrimers

Cangyi Chen,[†] Ping Tang,*[,†] Feng Qiu,*[,†] and An-Chang Shi[‡]

[†]The State Key Laboratory of Molecular Engineering of Polymers, Key Laboratory of Computational Physical Sciences, Department of Macromolecular Science, Fudan University, Shanghai 200433, China

[‡]Department of Physics and Astronomy, McMaster University, Hamilton, Ontario, Canada L8S 4M1

Supporting Information

**ABSTRACT:** The conformation of homodendrimers and amphiphilic dendrimers in various solvents is studied using classical density functional theory (DFT), in which the excluded-volume effects are treated explicitly. For homodendrimers in an athermal solvent, DFT results predict a remarkable fold-back behavior for the outer generation of segments, supporting the dense-core model. A coil-to-globule transition is observed for homodendrimers in a poor solvent. The size of the dendrimers, characterized by the radius of gyration, $\langle R_g \rangle$, is found to follow the scaling relationship, $\langle R_g \rangle \sim N^{\nu}$, where $N$ is the total number of segments of the dendrimers. For amphiphilic dendrimers, DFT results show that chemical modification in the outermost generation is an effective method to drive the ends toward the periphery of the dendrimers. In particular, a conformation with a hollow interior structure could be formed for amphiphilic dendrimers with longer end spacers in a selective solvent. The resulting unimolecular micelles with a hollow core and dense shell could serve as a unique candidate for encapsulation applications, such as sustained-drug-release nanocontainers.

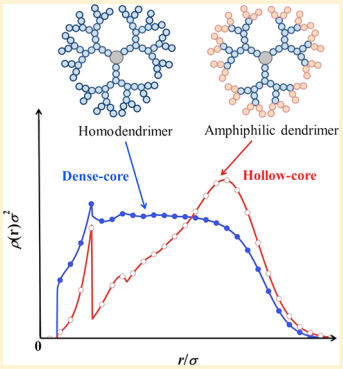


## 1. INTRODUCTION

Dendrimers are regularly branched macromolecules consisting of polymer chains originating from a central core.[1−3] Recent developments in synthetic chemistry have resulted in efficient methods to obtain highly monodisperse dendrimers with well-defined architectures.[4−6] In general, the conformation of dendrimers in solution is controlled by a number of characteristics, including the number of generations, degree of functionality, length of spacers, and property of terminal groups. In particular, the terminal groups of dendrimers could possess different appearances,[7,8] chemical natures,[9,10] or charges.[11,12] Because of the diversity in these features, the study of dendrimers has attracted tremendous attention, due to their importance in fundamental polymer physics and potential applications including chemical catalysis, hierarchical organization, drug delivery, biological applications, etc.[13−17]

Among the many properties of dendrimers, understanding their conformation, or internal structure, provides a foundation for the development of applications using dendrimers. Although various theoretical and simulation studies have been devoted to the prediction of the internal structure of isolated dendrimers,[18−32] it has been argued in the literature whether an isolated dendrimer possesses a dense or hollow shell. The dense-shell model was first suggested by de Gennes and Hervet in a pioneering theoretical work.[18] They considered a trifunctional dendrimer with very long flexible spacers in an athermal solvent. Using an analytical self-consistent field (SCF) approach, they found that the segment density increases from the center to the periphery monotonically. A crucial assumption in their theoretical model is that each subsequent generation lies at a further radial distance from the center of the dendrimer. Under this assumption, the free ends would locate at the outermost surface of the molecule. Their results implied that dendrimers with their hollow-core feature could be used as containers for drug, dye, or metal nanoparticles.

However, an opposite conclusion was made in subsequent computer simulations and theoretical studies. Lescanec and Muthukumar[19] first performed a numerical simulation of dendrimers using a kinetic growth algorithm of self-avoiding walks. In contrast to the results of de Gennes and Hervet,[18] they observed that the density decreases outward from the center monotonically, and the free ends are distributed throughout the molecule. This dense-core structure is further supported by subsequent Monte Carlo (MC)[20,22] and molecular dynamics (MD)[23,24] simulations. Experimentally, small-angle X-ray scattering and small-angle neutron scattering are the most powerful tools to elucidate the spatial structure of dendrimers in dilute solvents. Since Bauer et al.[33] first applied these methods to investigate the structure of dissolved dendrimers, a number of experimental results have provided evidence to support the dense-core model.[34−36] Despite these studies, the dense-core model has not been fully accepted in some cases.[37−39]

**Received:** March 23, 2016
**Revised:** May 12, 2016
**Published:** May 31, 2016






DOI: 10.1021/acs.jpcb.6b03005
J. Phys. Chem. B 2016, 120, 5553−5563

The first theoretical study supporting the dense-core model was performed by Boris and Rubinstein.[21] In comparison with the model of de Gennes and Hervet,[18] there are no prior assumptions about the distribution of the generations in the SCF calculation of Boris and Rubinstein. By incorporating the excluded-volume interaction within the self-consistent density field, the configuration of a dendrimer is determined by the balance between the chain entropy and excluded-volume interaction. Despite an overall dense-core picture predicted by Boris and Rubinstein, there are still some differences between the SCF theory (SCFT) results and simulations. In particular, the excluded-volume interactions in the SCF framework include only the two-body interactions derived from Flory theory. Although this approach is valid in most cases, Flory theory neglects three-body and higher excluded-volume interactions, so significant deviations should be expected in cases in which excluded-volume energy plays a major role. For trifunctional dendrimers, the number of segments grows exponentially with the number of generations. Hence, strong local crowding and dominance of excluded-volume effects are expected in dendrimers. This situation is similar to that of polymer brushes with high grafting densities or at very high compressions.[40−43] In that case, SCFT of Milner et al.[40] with two-body interactions also underestimated the excluded-volume effects, and deviations from the SCF predictions of brush structure were found in MD simulations.[41,42]

In the current work, we develop a classical density functional theory (DFT) to investigate the internal structure of an isolated dendrimer in explicit solvents. The DFT approach has proven to be a valid theoretical approach for systems with strong excluded-volume interactions.[43] On the basis of a hard-sphere chain model, DFT can treat the fine details of the excluded-volume effects between the segments or solvents explicitly. Other than hard-sphere interactions, we also introduce van der Waals interactions to study the properties of dendrimers under varying solvent conditions. The DFT approach is applied to homodendrimers and amphiphilic dendrimers. As many technological applications of dendrimers require a dense-shell structure, it is necessary to design such a structure by including extra interactions. The methods to control the structure include adding rigid spacers or charges or chemical modification. Among these methods, chemical modification on the periphery is considered to be a simple and effective way because the number of accessible end groups grows exponentially with generation.[9,44−48] For this reason, amphiphilic dendrimers are designed to control the spatial distribution of segments in this work. We will demonstrate that the modified free ends of dendrimers could lead to the formation of dense-shell structures, thus providing a potential candidate for encapsulation applications, such as drug, dye, or metal nanoparticles.

The remainder of this paper is organized as follows. Section 2 introduces the molecular models and strategy to obtain the distribution of segments of an isolated dendrimer under a DFT framework. Section 3 describes the key equations of DFT and the numerical method for a dendritic molecule in a spherical coordinate. Section 4 presents the numerical results and corresponding discussion. Section 5 summarizes the main results.

## 2. MOLECULAR MODELS

We consider an isolated homodendrimer or amphiphilic dendrimer in explicit solvents. Schematic diagrams of these model molecules are shown in Figure 1. Consistent with the literature, both the number of regularly branched dendrons and

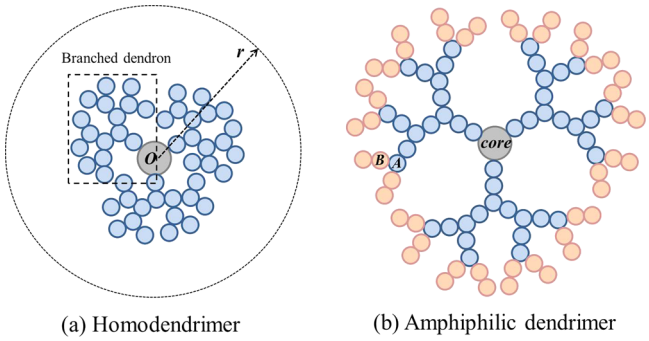


(a) Homodendrimer (b) Amphiphilic dendrimer

**Figure 1.** Schematic diagram of dendrimer models: (a) isolated homodendrimer with $G = 4$, $M_S = 1$; (b) isolated amphiphilic dendrimer with $G = 4$, $M_S = 2$. The symbol $r$ denotes the radial distance from a spherical shell to the core in a spherical coordinate, in which the origin is fixed at the center of the core. The inner gray sphere represents the core of the dendrimers. The blue and red spheres represent different segments for an amphiphilic dendrimer, respectively.

functionality of each branch point are fixed at $F_C = 3$. A coarse-grained model is employed to represent the dendrimers, in which the segments are modeled as freely jointed hard spheres with diameter $\sigma_D$. The number of generations and segments in each spacer are denoted as $G$ and $M_S$, respectively. The total number of segments in a dendrimer can be calculated by $N = F_C \times N_D$, where $N_D$ is the number of segments in each branched dendron as $N_D = M_S \times (2^G - 1)$. We exploit the spherical symmetry of the dendrimer and use a spherical coordinate system to describe the spatial distribution of segments. The number density is assumed to be uniformly distributed within a spherical shell at given radial distance $r$ from the core. The conformation of the dendrimer can be conveniently described by radial segment density $\rho(r)$.

The homodendrimer or amphiphilic dendrimer is immersed in solvent S modeled as hard spheres. For an amphiphilic dendrimer, the chemical nature of the segments in the outermost generation are distinguished from that of those in the inner generations, which are marked as A and B in Figure 1b. We assume that these different segments and solvent molecules are hard spheres with the same size ($\sigma_A = \sigma_B = \sigma_S = \sigma$). The pair interactions between them are described by a square-well (SW) potential[49]

$$\varphi_{ij}(r_{ij}) = \begin{cases} \infty, & r_{ij} < \sigma \\ -\varepsilon_{ij}, & \sigma \le r_{ij} \le \gamma\sigma \\ 0, & r_{ij} > \gamma\sigma \end{cases} \quad (1)$$

where $r_{ij}$ and $\varepsilon_{ij}$ are the distance and interaction strength, respectively, between segments $i$ and $j$ ($i, j$ = A, B, or S) and $\gamma\sigma$ is the SW width. Throughout this work, the width of the potential well is fixed at $\gamma = 1.5$. Furthermore, we set $\varepsilon_{AA} = \varepsilon_{BB} = \varepsilon_{SS} = \varepsilon$, and the reduced energy is defined as $\varepsilon^* = \varepsilon/k_BT$. Besides hard-core repulsion, attractive pair interactions exist within the SW width between the same species (e.g., AA, BB, or SS). According to the above definition, the athermal solvent condition mentioned in this work means that the interaction strength between the segments and solvents is $\varepsilon_{AS} = \varepsilon_{BS} = \varepsilon$, which could be considered as one kind of good solvent. In


DOI: 10.1021/acs.jpcb.6b03005
J. Phys. Chem. B 2016, 120, 5553−5563

contrast, if the solvents tend to repel the segments within the SW width, the interaction strength between them, $\varepsilon_{iS}(i = A,B)$, should be smaller than that between the same species, $\varepsilon$. In this work, we choose $\varepsilon_{AS} = \varepsilon_{BS} = 0$ to represent the poor solvent condition. The same definitions apply to the van der Waals interactions between segments A and B in the amphiphilic dendrimers.

It is instructive to view an isolated dendrimer as a grafting system in which the branched dendrons are tethered onto a spherical core. Taking advantage of this analogue, the internal structure of isolated dendrimers could be investigated within a DFT framework. We only need to calculate the probability distribution of a single branched dendron in the presence of a mean density field originating from all segments in the dendrimer. Within this description, the number of regularly branched dendrons is determined by grafting density $\rho_g\sigma_D^2$ and diameter of the spherical core $\sigma_C$ (i.e., $F_C = \pi\sigma_C^2\rho_g$). In the current work, the diameter of the core for a trifunctional dendrimer is chosen as $\sigma_C = 2\sigma_D$, representing the case of a moderate grafting density.

## 3. THEORETICAL DETAILS

**3.1. DFT.** The generic DFT equations and their numerical implementations have been reported in a number of previous publications.[50−53] Within the DFT framework, the Helmholtz free energy functional is conveniently expressed as an ideal gas contribution and an excess contribution accounting for intra- and intermolecular interactions

$$F[\rho_D(\boldsymbol{R}), \rho_{sol}(\boldsymbol{r})] = F_{id}[\rho_D(\boldsymbol{R}), \rho_{sol}(\boldsymbol{r})] + F_{ex}[\rho_D(\boldsymbol{R}), \rho_{sol}(\boldsymbol{r})] \tag{2}$$

where $\rho_D(\boldsymbol{R})$ is a multidimensional density profile and $\boldsymbol{R} \equiv (r_1, ..., r_N)$ is a set of coordinates describing the positions of segments in a dendrimer. For mixtures of hard-sphere solvents and dendrimers with bonding potentials, the ideal gas part of Helmholtz free energy is exactly known as

$$\beta F_{id}[\rho_D(\boldsymbol{R}), \rho_{sol}(\boldsymbol{r})] = \int d\boldsymbol{R}\rho_D(\boldsymbol{R})[\ln \rho_D(\boldsymbol{R}) - 1] + \beta\int d\boldsymbol{R}\rho_D(\boldsymbol{R})V_b(\boldsymbol{R}) + \int d\boldsymbol{r}\rho_{sol}(\boldsymbol{r})[\ln \rho_{sol}(\boldsymbol{r}) - 1] \tag{3}$$

where $V_b(\boldsymbol{R})$ is the direct bond potential. $\beta = 1/k_BT$, where $k_B$ is the Boltzmann constant and $T$ is the absolute temperature. As shown in the molecular models, the first segment of a branched dendron is tangentially tethered to the spherical core so that bonding potential $V_b(\boldsymbol{R})$ is specified by

$$\exp[-\beta V_b(\boldsymbol{R})] = k\delta\left(r_1 - \frac{\sigma_C + \sigma_D}{2}\right)\prod_{i\leftrightarrow j}\delta(|\boldsymbol{r}_i - \boldsymbol{r}_j| - \sigma_D) \tag{4}$$

where $r_1$ is the radial distance between the center of the tethered segment and core, $\delta$ is the Dirac-delta function, and $k$ is the normalization constant.

The key assumption in polymeric DFT is that the excess Helmholtz free energy functional can be accounted for using only segment densities.[50] The number density of the total segments, $\rho_D(\boldsymbol{r})$, and the local density of a particular segment, $\rho_{s,i}(\boldsymbol{r})$, are introduced via

$$\rho_D(\boldsymbol{R}) = \rho_A(\boldsymbol{r}) + \rho_B(\boldsymbol{r})$$
$$\rho_{s=A,B}(\boldsymbol{r}) = \sum_{i=1}^{N_s}\rho_{s,i}(\boldsymbol{r}) = \sum_{i=1}^{N_s}\int d\boldsymbol{R}\delta(\boldsymbol{r} - \boldsymbol{r}_i)\rho_D(\boldsymbol{R}) \tag{5}$$

where $\rho_A(\boldsymbol{r})$ and $\rho_B(\boldsymbol{r})$ represent the densities of segments A and B, respectively, for an amphiphilic dendrimer. The excess part of Helmholtz free energy can be decomposed as contributions from hard-sphere repulsion, chain connectivity, and van der Waals attractions

$$\beta F_{ex}[\rho_A(\boldsymbol{r}), \rho_B(\boldsymbol{r}), \rho_{sol}(\boldsymbol{r})] = \beta F_{ex}^{hs} + \beta F_{ex}^{chain} + \beta F_{ex}^{att} \tag{6}$$

The hard-sphere repulsion of the excess Helmholtz free energy can be represented by

$$\beta F_{ex}^{hs} = \int d\boldsymbol{r}[-n_0\ln(1 - n_3) + \frac{n_1n_2 - \mathbf{n}_{V_1}\cdot\mathbf{n}_{V_2}}{1 - n_3} + \frac{[n_3 + (1 - n_3)^2\ln(1 - n_3)](n_2^3 - 3n_2\mathbf{n}_{V_2}\cdot\mathbf{n}_{V_2})}{36\pi n_3^2(1 - n_3)^2}] \tag{7}$$

where $n_\alpha(\mathbf{r})$ ($\alpha$ = 0, 1, 2, 3, $V_1$, $V_2$) are the scalar and vector weighted densities defined by[54]

$$n_\alpha(\boldsymbol{r}) = \sum_j n_{\alpha j}(\boldsymbol{r}) = \sum_j\int\rho_j(\boldsymbol{r}')w_{\alpha j}(\boldsymbol{r} - \boldsymbol{r}')\,d\boldsymbol{r}' \tag{8}$$

Here, $w_{\alpha j}$ ($\alpha$ = 0, 1, 2, 3, $V_1$, $V_2$) are six weight functions and $j$ stands for segment A or B or solvent S. The excess Helmholtz free energy due to chain connectivity is evaluated on the basis of a first-order thermodynamic perturbation theory[55]

$$\beta F_{ex}^{chain} = \int d\boldsymbol{r}\frac{1 - N_D}{N_D}n_{0D}\xi_D\ln y_{11}^{hs}(\sigma_D, n_\alpha) \tag{9}$$

In the above, $\xi_D = 1 - \mathbf{n}_{V_{2D}}\cdot\mathbf{n}_{V_{2D}}/n_{2D}^2$, and $y_{11}^{hs}(\sigma_D, n_\alpha)$ is given by

$$y_{11}^{hs}(\sigma_D, n_\alpha) = \frac{1}{1 - n_3} + \frac{n_2\sigma_D\zeta}{4(1 - n_3)^2} + \frac{n_2^2\sigma_D^2\zeta}{72(1 - n_3)^3} \tag{10}$$

with $\xi = 1 - \mathbf{n}_{V_2}\cdot\mathbf{n}_{V_2}/n_2^2$. Finally, the excess Helmholtz free energy due to van der Waals attractions is represented by a mean field approximation[56]

$$\beta F_{ex}^{att} = \frac{1}{2}\iint d\boldsymbol{r}\,d\boldsymbol{r}'\sum_{i,j=A,B,S}\rho_i(\boldsymbol{r})\rho_j(\boldsymbol{r}')\varphi_{ij}(|\boldsymbol{r} - \boldsymbol{r}'|) \tag{11}$$

The grand potential functional is related to the Helmholtz free energy functional by a Legendre transformation

$$\Omega[\rho_D(\boldsymbol{R}), \rho_{sol}(\boldsymbol{r})] = F[\rho_D(\boldsymbol{R}), \rho_{sol}(\boldsymbol{r})] + \int[\psi_D(\boldsymbol{R}) - \mu_D]\rho_D(\boldsymbol{R})\,d\boldsymbol{R} + \int[\psi_{sol}(\boldsymbol{r}) - \mu_{sol}]\rho_{sol}(\boldsymbol{r})\,d\boldsymbol{r} \tag{12}$$

where $\mu_D$ and $\mu_{sol}$ are the chemical potentials of the grafted dendrons and hard-sphere solvents, respectively. $\psi_D(\boldsymbol{R})$ and $\psi_{sol}(\boldsymbol{r})$ are the external potentials exerting on individual segments and solvents, respectively. Minimization of the grand potential yields a set of Euler−Lagrange equations


DOI: 10.1021/acs.jpcb.6b03005
J. Phys. Chem. B 2016, 120, 5553−5563

$$\rho_D(\boldsymbol{R}) = \exp\left[\beta\mu_D - \psi_D(\boldsymbol{R}) - \beta V_b(\boldsymbol{R}) - \frac{\delta\beta F_{ex}}{\delta\rho_A(\boldsymbol{r})} - \frac{\delta\beta F_{ex}}{\delta\rho_B(\boldsymbol{r})}\right] \quad (13)$$

$$\rho_{sol}(\boldsymbol{r}) = \exp\left[\beta\mu_{sol} - \psi_{sol}(\boldsymbol{r}) - \frac{\delta\beta F_{ex}}{\delta\rho_{sol}(\boldsymbol{r})}\right] \quad (14)$$

**3.2. Numerical Methods.** For dendritic polymers, the key issue to solve eq 13 is to simplify complex direct bonding connectivity $V_b(\boldsymbol{R})$. The branched dendron can be considered as a tree-type structure.[57] Each free end has an equivalent path with length $N_{path} = G \times N_S$ to the core. The segments that locate at the same position along the path are considered to be equivalent. Two propagator functions, $G^i_{gra}(r)$ and $G^i_{free}(r)$, are defined to represent the connectivity of the path starting from the grafted segment and free end, respectively (as shown in Figure 2). In particular, we need to calculate the accumulated weight due to the direct bonding connectivity at each branch point (marked as yellow spheres in Figure 2).

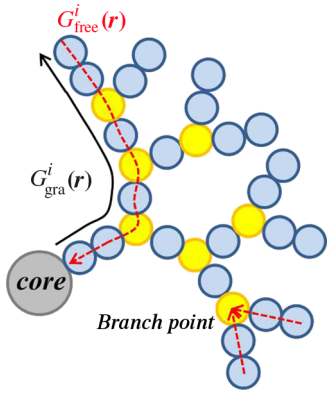


**Figure 2.** Schematic diagram for simplifying complex direct bonding connectivity $V_b(\boldsymbol{R})$ of each branched dendron. Two propagator functions, $G^i_{gra}(r)$ (black solid line) and $G^i_{free}(r)$ (red dashed line), are defined to represent the connectivity of one end-to-core path, respectively. The branch points are marked in yellow. Here, the intersection of arrows means an accumulated propagator should be considered.

For spherical coordinate systems with density profiles varying in only the radial direction, the two propagators are determined from the following recurrence relations

$$G^i_{gra}(r) = \frac{1}{2\sigma_D r}\int_0^\infty r'\,dr'\,\exp[-\beta\lambda_{i-1}(r')]G^{i-1}_{gra}(r')\,\theta(\sigma_D - |r - r'|) \quad (15)$$

for $i = 3, ..., N_{path}$ with

$$G^2_{gra}(r) = \frac{\sigma_C + \sigma_D}{4\sigma_D r}\exp\left[-\beta\lambda_{i-1}\left(\frac{\sigma_C + \sigma_D}{2}\right)\right]\theta\left(\sigma_D - \left|r - \frac{\sigma_C + \sigma_D}{2}\right|\right) \quad (16)$$

and

$$G^i_{free}(r) = \frac{1}{2\sigma_D r}\int_0^\infty r'\,dr'\,\exp[-\beta\lambda_{i+1}(r')]G^{i+1}_{free}(r')\,\theta(\sigma_D - |r - r'|) \quad (17)$$

for $i = 1, ..., N_{path} - 1$ with $G^{N_{path}}_{free}(r) = 1$. Here, effective potential field $\lambda_i(r) = \delta F_{ex}/\delta\rho_j(r) + \psi_j(r)$ depends on the identity of segment $j$ (A or B). Furthermore, the accumulation rules of propagators in each branch point are expressed as

$$G^i_{free}(r) = G^i_{free}(r) \times G^i_{free}(r) \quad (18)$$

$$G^i_{gra}(r) = G^i_{gra}(r) \times G^{N_{path}-i+1}_{free}(r) \quad (19)$$

Combining with eq 5, the density distributions in eqs 13 and 14 can be simplified to

$$\rho_{A\,or\,B}(r) = k\,\exp(\beta\mu_D)\sum_{i=A,B}\{2^{g-1}\exp[-\beta\lambda_i(r)]G^i_{gra}(r)\,G^i_{free}(r)\} \quad (20)$$

$$\rho_{sol}(r) = \exp\left[\beta\mu_{sol} - \psi_{sol}(r) - \frac{\delta\beta F_{ex}}{\delta\rho_{sol}(r)}\right] \quad (21)$$

where $g$ represents the sequence number of generation from the core ($g = 1 \sim G$) and $2^{g-1}$ is the number of segments that locates at the same position along the end-to-core path.

Particularly, as the branched dendrons are grafted onto a spherical core, the density distribution of the tethered segments is given by

$$\rho_{s,1}(r) = \rho_g\delta\left(r - \frac{\sigma_C + \sigma_D}{2}\right) \quad (22)$$

Coefficient $k\,\exp(\beta\mu_D)$ in eq 20 can be considered as a constant, which is determined by the normalization condition applied to each segment

$$\rho_g = \frac{1}{(\sigma_C/2)^2}\int_0^\infty r^2\rho_{s,i}(r)\,dr \quad (23)$$

We solve eqs 15 and 17 using the conventional Picard iteration method.[50] The final results are obtained when the difference between the input and output for densities is smaller than 0.001. Numerical integrations are performed with a step size of $\Delta r = 0.01\sigma_D$.

To further test the justification of the dendrimer molecular model and approximation in our DFT calculation, we make a direct comparison with the MD simulation data of the homopolymer dendrimers in ref 24 (see Supporting Information). The DFT results are consistent with the corresponding MD data, with a slightly lower number density of the segment near the center (near $r = 1$ in Figure S1). Such weak differences in a narrow region are not important when discussing the conformation of a dendrimer. Furthermore, direct comparison shows that the excluded-volume interactions between the segments are more rigorously enforced in the DFT model.

## 4. RESULTS AND DISCUSSION

**4.1. Isolated Homodendrimer in Explicit Solvents.** First, we investigate the internal structure of an isolated homodendrimer in solvents with different qualities. For a homodendrimer in a solvent, there is only one type of segment, denoted as $D$. The conformation or internal structure of a


DOI: 10.1021/acs.jpcb.6b03005
J. Phys. Chem. B 2016, 120, 5553−5563

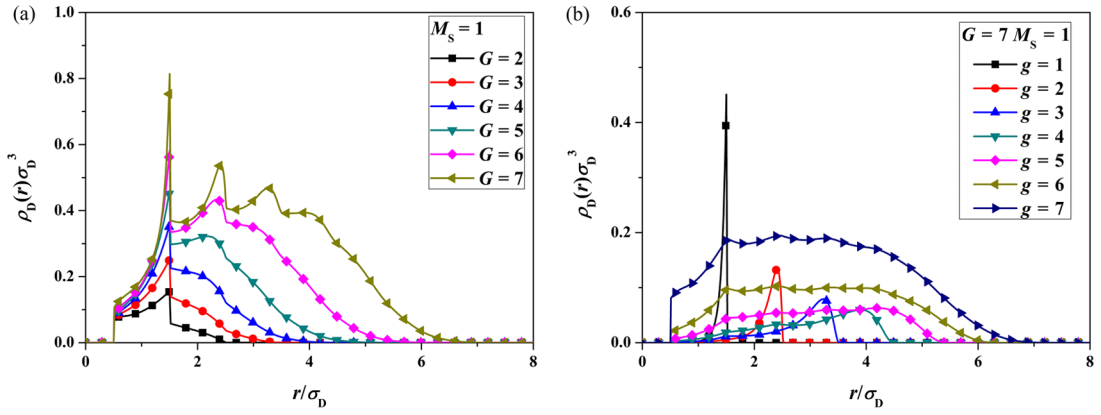


**Figure 3.** (a) Total segment density profiles $\rho_D(r)\sigma_D^3$ of homodendrimers with spacer length $M_S$ = 1 in an athermal solvent ($\varepsilon_{DS} = \varepsilon$) as a function of radial distance $r$. (b) Segment distributions in each generation of the homodendrimer, with $G$ = 7, $M_S$ = 1. For ease of description, the origin is shifted from the center of the core to the grafting surface in all density profiles.

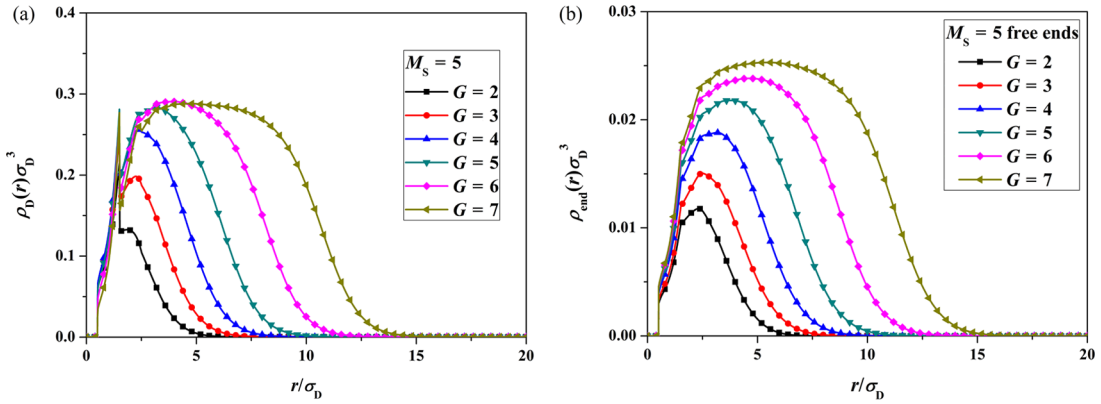


**Figure 4.** (a) Total segment density profiles $\rho_D(r)\sigma_D^3$ of homodendrimers with spacer length $M_S$ = 5 in an athermal solvent as a function of radial distance $r$. (b) Distributions of free ends $\rho_{end}(r)\sigma_D^3$ in the above dendrimers.

dendrimer depends on the number of generations, length of spacers, and interaction strength $\varepsilon_{DS}$ between segments and solvents. In what follows, the bulk density of the solvent is fixed at $\rho_{bulk\_S}\sigma_s^3$ = 0.20, unless denoted otherwise.

*4.1.1. Athermal Solvent.* Figure 3a shows the radial segment density profiles of homodendrimers with spacer length $M_S$ = 1 in an athermal solvent ($\varepsilon_{DS} = \varepsilon$) when the number of generations increases from $G$ = 2 to 7. The first feature to notice is that the dense-shell picture suggested by de Gennes and Hervet[18] is not supported by the DFT results. Ordered segment shells can be observed in the radial density profiles of dendrimers with high generations. For example, the density distribution of segments shows three obvious ordered shells located at $r/\sigma_D$ = 1.5, 2.4, 3.2 for $G$ = 7 in Figure 3a. These ordered shells reveal that the segments in the inner generations have layered arrangements. This conclusion is supported by the segment distributions of each generation shown in Figure 3b. Here, these ordered arrangements in the dendrimers with high generations originate from the strongly excluded-volume interactions between the segments. Note that the dendrimer with a short spacer, $M_S$ = 1, is a special topological structure known as Cayley tree,[19] in which each generation is closely linked together (see Figure 1a). The segments in the inner generations do not have enough space to adjust the conformation, thus they tend to line up along the radial direction. However, a remarkable fold-back behavior can be found in the outer generations. Because of fold-backing, no obvious segment aggregation occurs in generations $g$ = 5−7 for $G$ = 7.

The DFT results shown in Figure 3 present a detailed picture of the short-range internal structure of a Cayley tree case. On the other hand, the theoretical predications of Boris and Rubinstein[21] are valid for long spacers, so it is necessary to extend the DFT results to cases with longer spacers. Figure 4 presents the segment density profiles of homodendrimers with spacer length $M_S$ = 5 in an athermal solvent. A dense-core picture can be clearly seen for all cases in Figure 4a. Furthermore, the distribution of the free ends shown in Figure 4b covers the whole dendritic molecule. This result indicates that the ends of the dendrimer are not restricted to the surface because of the effect of the conformation entropy. Meanwhile, they are also difficult to fold back into the region near the core of the dendrimer in which the excluded-volume interactions are remarkable, so we observe that the free ends aggregate in the middle region between the core and outermost surface. Thus, the configuration of the dendrimer is a result of the balance between the excluded-volume interaction and entropy. The general features of dendrimers with longer flexible spacers are in agreement with the results of SCFT.[21] However, unlike a monotonically decreasing density profile in SCFT, we find that in each of the density profiles there exists a local density minimum at a small radial distance (Figure 4a). Then, an almost constant density zone is apparent, starting from the local density minimum. The plateau zone expands with an increase



DOI: 10.1021/acs.jpcb.6b03005
J. Phys. Chem. B 2016, 120, 5553−5563

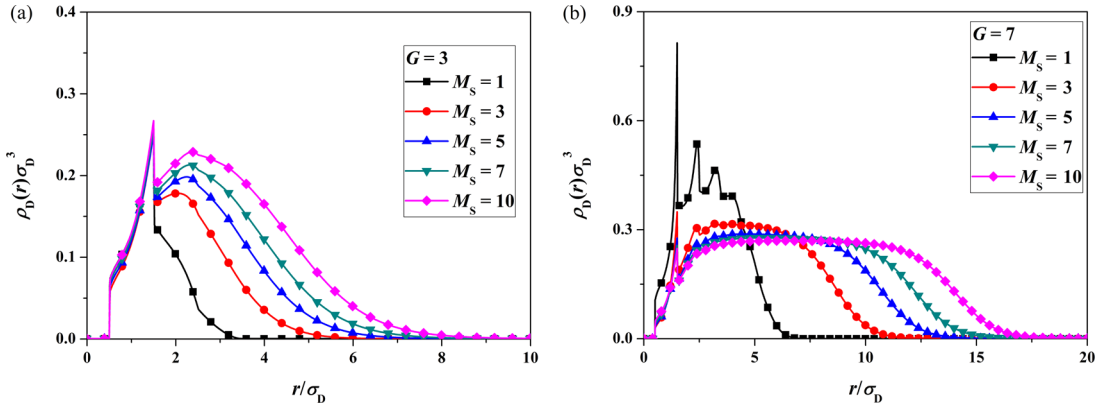


**Figure 5.** Segment density profiles of dendrimers with different spacer lengths ($M_S$ = 1, 3, 5, 7, 10) for two typical generations: (a) $G$ = 3; (b) $G$ = 7.

in generations but barely exists for the $G$ = 4 dendrimer. Beyond this plateau region, each density profile in the tail zone is smooth and decreases monotonically to zero. These details revealed by the DFT results are qualitatively similar to those found by the MC and MD simulations.[20,23]

As shown above, instead of the ordered shells observed in the Cayley tree case, a constant density zone occurs as the spacer length increases to $M_S$ = 5. Obviously, the spacer length has a significant effect on the structure of the dendrimers. To discuss this effect in detail, the density profiles of $G$ = 3 and 7 dendrimers with different spacer lengths ($M_S$ = 1, 3, 5, 7, 10) are presented in Figure 5a,b, respectively. As the spacer length increases, the segment density of the $G$ = 3 dendrimer in Figure 5a always increases at given distance $r/\sigma_D$. As the generation in this case is small, the segments are much easier to fold back for a dendrimer with a longer spacer; then, the fold-backing segments make the density increase at the region near the core. However, an opposite phenomenon is seen for the $G$ = 7 dendrimer in Figure 5b. At the region near the core, we find that the segment density decreases with an increase in the spacer length at given distance $r/\sigma_D$. This behavior could be attributed to the existence of an obvious dense-core plateau zone for $G$ = 7. The excluded-volume effects in the constant density zone will hinder the peripheral segments from penetrating into the inner region. As shown in Figure 5b, the plateau zone expands with an increase in spacer length. For this reason, a shorter spacer is much easier to penetrate into the region near the core in comparison with a long spacer.

*4.1.2. Coil-to-Globule Transition in a Poor Solvent.* In this section, we consider the conformation of homodendrimers in a poor solvent. Figure 6 shows the density profiles of segments $\rho_D(r)\sigma_D^3$ and solvents $\rho_S(r)\sigma_S^3$ for homodendrimers with $M_S$ = 5, $G$ = 6, in a poor solvent ($\varepsilon_{DS}$ = 0). As a comparison, the density profiles of the same dendrimer immersed in an athermal solvent ($\varepsilon_{DS}$ = $\varepsilon$) are also shown. The results demonstrate that the dendrimer undergoes a collapse transition in the poor solvent. A more dense constant density zone appears in the segment density profile, and the interface between the dendrimer and solvents becomes sharper. It should be noted that previous simulations[23,29] predicted that dendrimers always behave as compact space-filling objects even in an athermal solvent. However, the current DFT results show that although the segments are crowded in some local region considerable void spaces are available in the whole dendrimer. This conclusion is supported by the distribution of athermal solvents in Figure 6 (red line with open symbol), in which the solvents penetrate

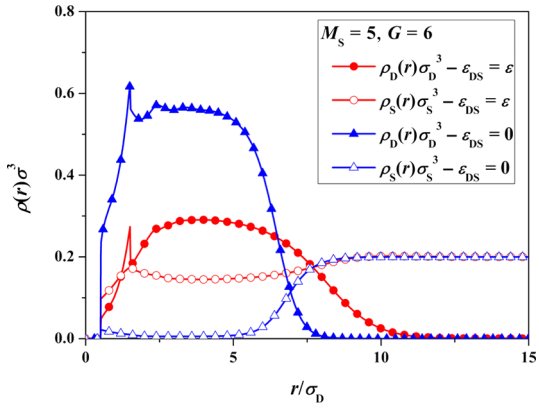


**Figure 6.** Density profiles of segments $\rho_D(r)\sigma_D^3$ and solvents $\rho_S(r)\sigma_S^3$ for homodendrimers with $M_S$ = 5, $G$ = 6, in an athermal solvent ($\varepsilon_{DS}$ = $\varepsilon$) and poor solvent ($\varepsilon_{DS}$ = 0).

throughout the dendrimer. Because of the existence of available void spaces, a coil-to-globule transition can be observed when the solvent quality changes from athermal to poor. On the basis of the blue line with open symbols in Figure 6, we note that in the collapsed state almost all of the poor solvents are excluded from the dendrimers. These results suggest that solvent quality is an efficient factor to regulate the morphology of homodendrimers, which is important for the application of dendrimers in various environments.

The collapse behavior of dendrimers can be directly reflected by the change in dendrimer size. We calculate radius of gyration $\langle R_g \rangle$ of a dendrimer by

$$\langle R_g \rangle = \left( \frac{\int \mathrm{d}r \rho_D(r) r^4}{\int \mathrm{d}r \rho_D(r) r^2} \right)^{1/2} \quad (24)$$

where the origin is assumed as the center of mass due to the spherical symmetry of the molecule. Furthermore, to compare the coil-to-globule transition with previous theoretical and experimental studies, we define collapse factor $f_{collapse} = \langle R_g^A \rangle / \langle R_g^P \rangle$ and average degree of filling inside the dendrimer $D_f = 3N b^3 / 4\pi R^3$, where $R$ is the apparent radius of the dendrimer. Radius of gyration $\langle R_g \rangle$, average degree of filling $D_f$, and the collapse factor for dendrimers with $M_S$ = 5 in athermal ($\varepsilon_{DS}$ = $\varepsilon$) and poor ($\varepsilon_{DS}$ = 0) solvents are listed in Table 1. It is seen that dendrimer size in a poor solvent is significantly smaller than that in an athermal solvent. In terms of average degree of filling $D_f$, the estimated value of $D_f$ = 0.15−0.17 in the athermal


DOI: 10.1021/acs.jpcb.6b03005
J. Phys. Chem. B 2016, 120, 5553−5563

**Table 1. Radius of Gyration $\langle R_g \rangle$, Average Degree of Filling $D_f$, and the Collapse Factor of Dendrimers with $M_S = 5$ in Athermal ($\varepsilon_{DS} = \varepsilon$) and Poor ($\varepsilon_{DS} = 0$) Solvents**

| | | $\langle R_g \rangle$[b] | | $D_f$ | | |
|---|---|---|---|---|---|---|
| $G$[a] | $N$ | $\langle R_g^A \rangle$ | $\langle R_g^P \rangle$ | athermal | poor | $f_{collapse}$ |
| 2 | 45 | 3.18 | 2.83 | 0.15 | 0.22 | 1.12 |
| 3 | 105 | 4.08 | 3.35 | 0.17 | 0.31 | 1.22 |
| 4 | 225 | 5.01 | 3.60 | 0.17 | 0.40 | 1.39 |
| 5 | 465 | 6.15 | 4.52 | 0.17 | 0.46 | 1.36 |
| 6 | 945 | 8.86 | 5.97 | 0.16 | 0.49 | 1.45 |
| 7 | 1905 | 10.99 | 7.44 | 0.16 | 0.52 | 1.48 |

[a]Note that the number of generations may count from $G = 0$ in the literature.[23,27] [b]$\langle R_g^A \rangle$ and $\langle R_g^P \rangle$ represent the radii of gyration of dendrimers in athermal and poor solvents, respectively.

solvent supports the existence of available void spaces. This value is very close to the result of MC simulations.[29] In a poor solvent, average degree of filling $D_f$ shows a generation-dependence in our DFT results. Furthermore, the collapse factor of a dendrimer with $G = 2$ is smaller than that of the high-generation cases, which means no significant collapse occurs in the low-generation dendrimers. This behavior is also captured in previous experiments.[58,59] A detailed comparison between the previous theoretical and experimental data can be seen in ref 29, but there are no definitive conclusions due to the differences in the definition of solvent quality and the coarse-graining details in these works.[23,26,29,58,59]

*4.1.3. Scaling Behavior: $\langle R_g \rangle$ versus N.* Most of the previous theoretical and experimental studies have shown a power-law behavior of the dendrimer's size as a function of the number of segments, spacer length, or generation number.[12,18−29] Figure 7

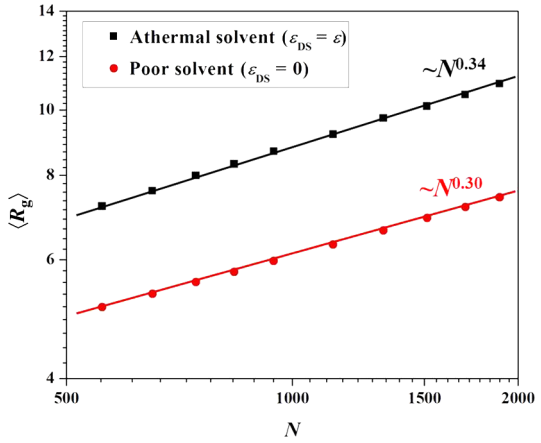


**Figure 7.** Variation of radius of gyration $\langle R_g \rangle$ as a function of total number of segments $N$ on a double-logarithmic scale. The black and red points are calculated from the data corresponding to the dendrimers with relatively large $N$ in an athermal solvent and poor solvent, respectively. The solid lines are the best linear fit of the form $\langle R_g \rangle \sim N^{\nu}$.

shows variation of $\langle R_g \rangle$ as a function of total number of segments $N$ on a double-logarithmic scale. These points are calculated from the data corresponding to the dendrimers with relatively large $N$ in an athermal solvent (black) or poor solvent (red). Although a part of previous work has obtained various scaling laws, we can still find a simple relationship between $\langle R_g \rangle$ and $N$ with the form $\langle R_g \rangle \sim N^{\nu}$ in this work. The value of $\nu$ is 0.34 for the athermal solvent condition and 0.30 for the poor solvent condition. This result is consistent with the MD study of Murat and Grest[23] ($\nu = 0.30$ for both athermal and poor solvents) and the MC simulation of Giupponi and Buzzap ($\nu = 0.33$ and 0.32 for athermal and poor solvents, respectively).[29]

**4.2. Isolated Amphiphilic Dendrimer in Solvents.** Similar to most previous studies, our DFT results presented in the above section reveal a dense-core structure of homodendrimers. On the other hand, applications of dendrimers, such as in drug delivery and chemical catalysis, require a hollow interior or dense-shell structure. The idea of obtaining a dendrimer with a dense-shell structure by chemical end-group modification appears naturally because the number of end groups grows exponentially with generation. In this section, we will examine the structure of an amphiphilic dendrimer in nonselective and selective solvents. As shown in Figure 1b, segments B in the outermost generation of the amphiphilic dendrimer are chemically distinguished from segments A in the inner generations. We consider an amphiphilic dendrimer with a given generation $G = 5$ for simplicity.

*4.2.1. Amphiphilic Dendrimer in Nonselective Solvents.* Figure 8 shows the total density profiles and distributions of segments B of amphiphilic dendrimers with $M_S = 2$ in a nonselective poor solvent ($\varepsilon_{AS} = \varepsilon_{BS} = 0$). Here, the SW interaction strength between segments A and B changes from attractive ($\varepsilon_{AB} = \varepsilon$) to repulsive ($\varepsilon_{AB} = -\varepsilon$). As the repulsive interaction becomes stronger, we observe that the segment density near the core decreases, and the amphiphilic dendrimer extends outward as a whole. In the case of $\varepsilon_{AB} = -\varepsilon$, it is clear that segments B tend to aggregate near the dendrimer surface rather than having a uniform distribution in the inner space of the dendrimer at $\varepsilon_{AB} = \varepsilon$, as shown in Figure 8b. The result shows that the segregation between the two chemically different segments drives the ends to the periphery of end-modified amphiphilic dendrimers, resulting in a dense-shell structure. This observation is qualitatively in agreement with previous experimental and theoretical works.[60−64]

Figure 9 shows the density profiles of segments A and B as the spacer length increases to $M_S = 5$. In comparison with the amphiphilic dendrimer with a short spacer (Figure 8), a more remarkable density shell can be observed due to the strong aggregation of segments B at the periphery of the dendrimer. This result shows that a longer spacer is beneficial to form a denser shell. On the other hand, a similar dense-shell structure does not appear if the amphiphilic dendrimer is immersed in a nonselective good solvent. This phenomenon can be explained by referring to the mechanism of microphase separation in a diblock copolymer.[65] At the mean field level, the segregation of the chemically different segments is controlled by parameters $\chi N$ and $f$, where $\chi$ is the interaction parameter between the two components, $N$ is the effective chain length of the block copolymer, and $f$ is the volume fraction of one of the components. Unlike that for an amphiphilic dendrimer in a poor solvent, the penetrative good solvent will screen the effective interaction ($\chi$) between segments A and B, leading to a weak segregation between them. Similarly, the longer spacer length means a higher $\chi N$, which will promote segregation between segments A and B.

*4.2.2. Hollow-Core Structure in the Amphiphilic Dendrimer.* It is possible to realize the aggregation of end groups in the periphery of dendrimers by immersing the amphiphilic dendrimer in a nonselective poor solvent. However, the segments still have a high concentration near the center due


DOI: 10.1021/acs.jpcb.6b03005
J. Phys. Chem. B 2016, 120, 5553−5563

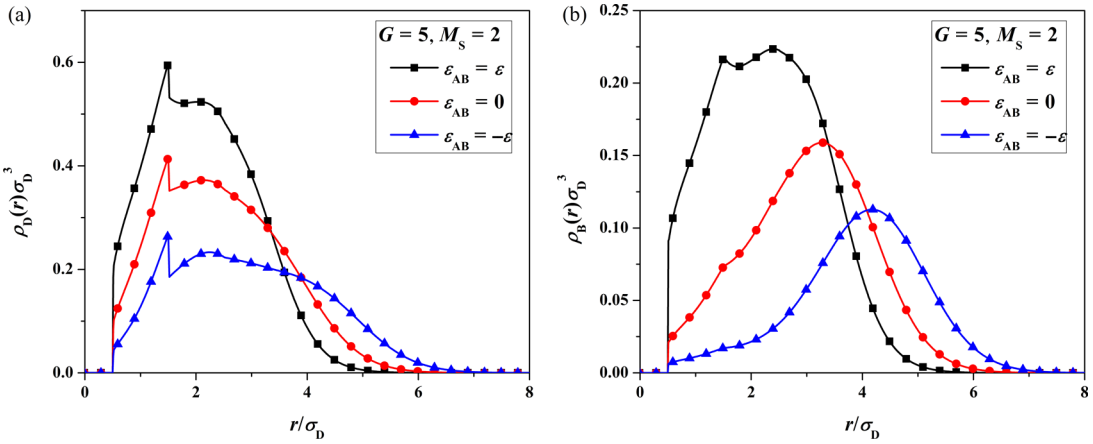


**Figure 8.** (a) Total density profiles and (b) distributions of segments B of an amphiphilic dendrimer with short spacer $M_S = 2$ in a nonselective poor solvent ($\varepsilon_{AS} = \varepsilon_{BS} = 0$). The SW interaction strength between segments A and B changes from attractive ($\varepsilon_{AB} = \varepsilon$) to repulsive ($\varepsilon_{AB} = -\varepsilon$).

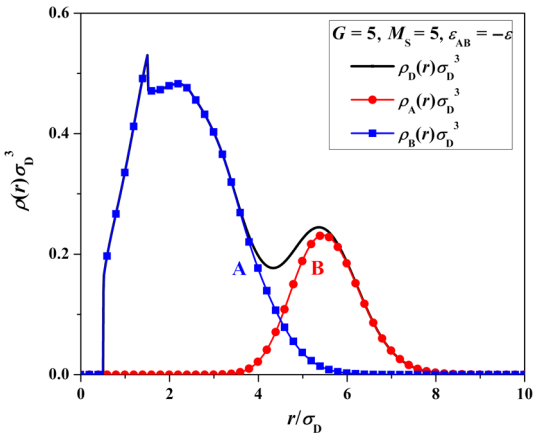


**Figure 9.** Density profiles of total segments (black line) and segments A and B (blue and red lines) when the spacer length of the amphiphilic dendrimer increases to $M_S = 5$. The solvent quality is the same as that in Figure 8.

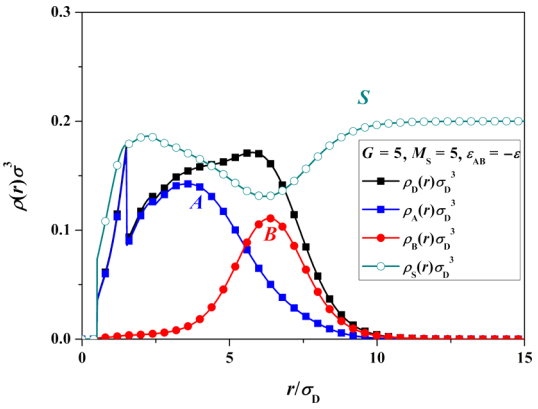


**Figure 10.** Density profiles of an amphiphilic dendrimer immersed in a selective solvent ($\varepsilon_{AS} = \varepsilon$, $\varepsilon_{BS} = 0$). Here, the total density of the dendrimer is shown as the black line. The distributions of segments A and B and solvents are shown as red, blue, and green lines, respectively.

to the collapse of dendrimers in a poor solvent. For this reason, we immerse the amphiphilic dendrimer in a selective solvent ($\varepsilon_{AS} = \varepsilon$, $\varepsilon_{BS} = 0$), in which segments A and B are solvophilic and solvophobic, respectively. The corresponding density profiles are shown in Figure 10. We observe that the solvents penetrate into the center of the dendrimer due to the existence of solvophilic segments A, which tend to extend into the solvent-rich area. On the other hand, solvophobic segments B guarantee segregation between A and B. As a consequence, we obtain a relatively hollow structure with a dense shell on the periphery of the dendrimer in Figure 10. Here, it should be noted that the drastic jump at $r/\sigma_D = 1.5$ in the segment number density originates from the grafting constraint. Apart from the drastic jump at this point, the result shows a well-defined dense-shell structure.

As mentioned above, segregation of the two chemically different segments will be influenced by volume fraction $f$. Inspired by this, we design a series of amphiphilic dendrimers with different spacer lengths on end generation $M_{end}$. The density profiles of these amphiphilic dendrimers in a selective solvent are shown in Figure 11. It is very interesting to observe that the hollow-core structure is much easier to obtain as the length of end spacers $M_{end}$ increases. In Figure 10a, when the end spacers, $M_{end} = 4$, are twice as long as the inner spacers, $M_S = 2$, a hollow interior is clearly visible. In this case, the number of segments B is almost twice as many as segments A. If the end spacers increase to larger than $M_{end} = 4$, then segments in the shell become denser. More interestingly, if both the inner and end spacers are long enough, we can observe a bimodal density distribution in the amphiphilic dendrimers (as shown in Figure 11b). In this unimolecular micelle, the solvents or other small molecules can permeate into the solvophilic interior easily, and the dense solvophobic shell can be seen as a covered protection layer. These results demonstrate that amphiphilic dendrimers possess the potential for applications requiring a controllable hollow-core structure, such as sustained drug release nanocontainers.[16,17]

## 5. CONCLUSIONS

We have introduced a classical DFT to describe the conformation, or internal structure, of isolated dendrimers in various explicit solvents. In comparison with the simple two-body interactions in classical analytic SCFT, our approach takes into account the excluded-volume effects between segments or solvents more accurately. Our DFT results support the dense-core model for homodendrimers in an athermal solvent, in agreement with most previous studies. In particular, we find an ordered-shell structure for the Cayley tree with high


DOI: 10.1021/acs.jpcb.6b03005
J. Phys. Chem. B 2016, 120, 5553−5563

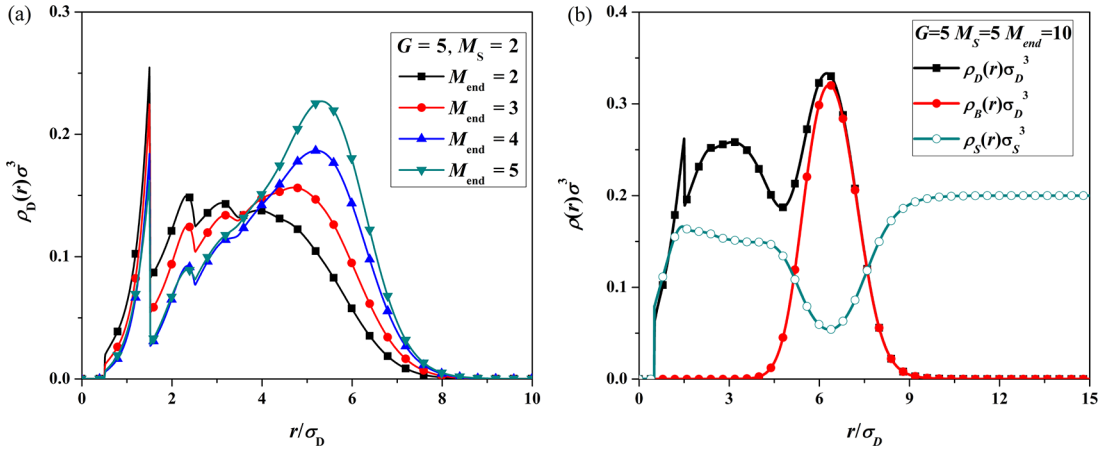


**Figure 11.** (a) Total segment density profiles of amphiphilic dendrimers ($M_S$ = 2) with different end spacer lengths, $M_{end}$ = 2−5. (b) Distribution of total segments, segments B, and solvents for amphiphilic dendrimers ($M_S$ = 5) with end spacers $M_{end}$ = 10. The amphiphilic dendrimers are immersed in the same selective solvent as that in Figure 10.

generations due to the strong topological excluded-volume effects. The influences of spacer length on inner structure have been investigated in detail. We observe a coil-to-globule transition when the homodendrimers are immersed in solvents with varying solvent qualities. The details of the collapse behavior are compared with those in previous theoretical and experimental works. For the power-law behavior of the dendrimer's size, we also find a simple scaling law between $\langle R_g \rangle$ and $N$, with a form $\langle R_g \rangle \sim N^{\nu}$, which is consistent with the computer simulation results.

We also designed an amphiphilic dendrimer in which the segments in the outermost generation are chemically distinguished from those in the inner generations. The results show that chemical modification of the outermost generation is an effective method to drive the ends to the periphery of the dendrimers. Aggregation of the segments in the periphery can be influenced by the interaction strength between two incompatible segments, spacer length, and solvent quality. More interestingly, we find that a hollow interior structure can be easily obtained for amphiphilic dendrimers with longer end spacers in a selective solvent. In these unimolecular micelles, the solvents or small molecules can permeate into the interior easily, and the dense solvophobic shell provides a covered protection layer. These amphiphilic dendrimers with dense shells have the potential to be used in sustained-drug-release applications.

## ■ ASSOCIATED CONTENT

### Supporting Information

The Supporting Information is available free of charge on the ACS Publications website at DOI: 10.1021/acs.jpcb.6b03005.

Further description on figures and tables regarding the comparison between the DFT and MD results (PDF)

## ■ AUTHOR INFORMATION

### Corresponding Authors

*E-mail: pingtang@fudan.edu.cn. Phone: 86-21-65642867 (P.T.).

*E-mail: fengqiu@fudan.edu.cn. Phone: 86-21-55664036 (F.Q.).

### Notes

The authors declare no competing financial interest.

## ■ ACKNOWLEDGMENTS

We gratefully acknowledge the financial support from the National Natural Science Foundation of China (Grant Nos. 21320102005 and 21374023). C.Y. Chen also acknowledges the financial support from the short-term international visiting scholar program of Fudan University. A.C.S. acknowledges the support from the Natural Sciences and Engineering Research Council (NSERC) of Canada.

## ■ REFERENCES

(1) Fischer, M.; Vogtle, F. Dendrimers: from design to application—a progress report. *Angew. Chem., Int. Ed.* **1999**, *38*, 884−905.

(2) Meijer, E. W.; van Genderen, M. H. P. Chemistry—dendrimers set to self-destruct. *Nature* **2003**, *426*, 128−129.

(3) Ballauff, M.; Likos, C. N. Dendrimers in solution: insight from theory and simulation. *Angew. Chem., Int. Ed.* **2004**, *43*, 2998−3020.

(4) Tomalia, D. A.; Baker, H.; Dewald, J.; Hall, M.; Kallos, G.; Martin, S.; Roeck, J.; Ryder, J.; Smith, P. A new class of polymers—Starburst-dendritic macromolecules. *Polym. J.* **1985**, *17*, 117−132.

(5) Hawker, C. J.; Frechet, J. M. J. A new convergent approach to monodisperse dendritic macromolecules. *J. Chem. Soc., Chem. Commun.* **1990**, *15*, 1010−1013.

(6) Dagani, R. Chemists explore potential of dendritic macromolecules as functional materials. *Chem. Eng. News* **1996**, *74*, 30−38.

(7) Genson, K. L.; Holzmueller, J.; Leshchiner, I.; Agina, E.; Boiko, N.; Shibaev, V. P.; Tsukruk, V. V. Organized monolayers of carbosilane dendrimers with mesogenic terminal groups. *Macromolecules* **2005**, *38*, 8028−8035.

(8) Jensen, A. W.; Maru, B. S.; Zhang, X.; Mohanty, D. K.; Fahlman, B. D.; Swanson, D. R.; Tomalia, D. A. Preparation of fullerene-shell dendrimer-core nanoconjugates. *Nano Lett.* **2005**, *5*, 1171−1173.

(9) Suek, N. W.; Lamm, M. H. Effect of terminal group modification on the solution properties of dendrimers: A molecular dynamics simulation study. *Macromolecules* **2006**, *39*, 4247−4255.

(10) Cao, W. Q.; Zhu, L. Synthesis and unimolecular micelles of amphiphilic dendrimer-like star polymer with various functional surface groups. *Macromolecules* **2011**, *44*, 1500−1512.

(11) Huissmann, S.; Likos, C. N.; Blaak, R. Effective interactions between charged dendrimers. *Soft Matter* **2011**, *7*, 8419−8427.

(12) Kłos, J. S.; Sommer, J. U. Simulations of neutral and charged dendrimers in solvents of varying quality. *Macromolecules* **2013**, *46*, 3107−3117.

(13) Bosman, A. W.; Janssen, H. M.; Meijer, E. W. About dendrimers: structure, physical properties, and applications. *Chem. Rev.* **1999**, *99*, 1665−1688.



DOI: 10.1021/acs.jpcb.6b03005
*J. Phys. Chem. B* 2016, 120, 5553−5563

(14) Crooks, R. M.; Zhao, M. Q.; Sun, L.; Chechik, V.; Yeung, L. K. Dendrimer-encapsulated metal nanoparticles: Synthesis, characterization, and applications to catalysis. *Acc. Chem. Res.* **2001**, *34*, 181−190.
(15) Percec, V.; Glodde, M.; Bera, T. K.; Miura, Y.; Shiyanovskaya, I.; Singer, K. D.; Balagurusamy, V. S. K.; Heiney, P. A.; Schnell, I.; Rapp, A.; Spiess, H. W.; Hudson, S. D.; Duan, H. Self-organization of supramolecular helical dendrimers into complex electronic materials. *Nature* **2002**, *417*, 384−387.
(16) Lee, C. C.; MacKay, J. A.; Frechet, J. M. J.; Szoka, F. C. Designing dendrimers for biological applications. *Nat. Biotechnol.* **2005**, *23*, 1517−1526.
(17) Kesharwani, P.; Jain, K.; Jain, N. K. Dendrimer as nanocarrier for drug delivery. *Prog. Polym. Sci.* **2014**, *39*, 268−307.
(18) de Gennes, P. G.; Hervet, H. Statistics of Starburst polymers. *J. Phys., Lett.* **1983**, *44*, L351−L360.
(19) Lescanec, R. L.; Muthukumar, M. Configurational characteristics and scaling behavior of Starburst molecules—a computational study. *Macromolecules* **1990**, *23*, 2280−2288.
(20) Mansfield, M. L.; Klushin, L. I. Monte-Carlo studies of dendrimer macromolecules. *Macromolecules* **1993**, *26*, 4262−4268.
(21) Boris, D.; Rubinstein, M. A self-consistent mean field model of a starburst dendrimer: dense core vs dense shell. *Macromolecules* **1996**, *29*, 7251−7260.
(22) Chen, Z. Y.; Cui, S. M. Monte Carlo simulations of star-burst dendrimers. *Macromolecules* **1996**, *29*, 7943−7952.
(23) Murat, M.; Grest, G. S. Molecular dynamics study of dendrimer molecules in solvents of varying quality. *Macromolecules* **1996**, *29*, 1278−1285.
(24) Karatasos, K.; Adolf, D. B.; Davies, G. R. Statics and dynamics of model dendrimers as studied by molecular dynamics simulations. *J. Chem. Phys.* **2001**, *115*, 5310−5318.
(25) Sheng, Y. J.; Jiang, S. Y.; Tsao, H. K. Radial size of a starburst dendrimer in solvents of varying quality. *Macromolecules* **2002**, *35*, 7865−7868.
(26) Timoshenko, E. G.; Kuznetsov, Y. A.; Connolly, R. Conformations of dendrimers in dilute solution. *J. Chem. Phys.* **2002**, *117*, 9050.
(27) Gotze, I. O.; Likos, C. N. Conformations of flexible dendrimers: a simulation study. *Macromolecules* **2003**, *36*, 8189−8197.
(28) Harreis, H. M.; Likos, C. N.; Ballauff, M. Can dendrimers be viewed as compact colloids? A simulation study of the fluctuations in a dendrimer of fourth generation. *J. Chem. Phys.* **2003**, *118*, 1979−1988.
(29) Giupponi, G.; Buzza, D. M. Monte Carlo simulation of dendrimers in variable solvent quality. *J. Chem. Phys.* **2004**, *120*, 10290−10298.
(30) Han, M.; Chen, P.; Yang, X. Molecular dynamics simulation of PAMAM dendrimer in aqueous solution. *Polymer* **2005**, *46*, 3481−3488.
(31) Freire, J. J.; Rubio, A. M. Conformational properties and Rouse dynamics of different dendrimer molecules. *Polymer* **2008**, *49*, 2762−2769.
(32) Klos, J. S.; Sommer, J. U. Properties of dendrimers with flexible spacer-chains: a Monte Carlo Study. *Macromolecules* **2009**, *42*, 4878−4886.
(33) Prosa, T. J.; Bauer, B. J.; Amis, E. J.; Tomalia, D. A.; Scherrenberg, R. A SAXS study of the internal structure of dendritic polymer systems. *J. Polym. Sci. Pol. Phys.* **1997**, *35*, 2913−2924.
(34) Potschke, D.; Ballauff, M.; Lindner, P.; Fischer, M.; Vogtle, F. Analysis of the structure of dendrimers in solution by small-angle neutron scattering including contrast variation. *Macromolecules* **1999**, *32*, 4079−4087.
(35) Prosa, T. J.; Bauer, B. J.; Amis, E. J. From stars to spheres: a SAXS analysis of dilute dendrimer solutions. *Macromolecules* **2001**, *34*, 4897−4906.
(36) Rosenfeldt, S.; Dingenouts, N.; Ballauff, M.; Werner, N.; Vogtle, F.; Lindner, P. Distribution of end groups within a dendritic structure: a SANS study including contrast variation. *Macromolecules* **2002**, *35*, 8098−8105.
(37) Uppuluri, S.; Keinath, S. E.; Tomalia, D. A.; Dvornic, P. R. Rheology of dendrimers. I. Newtonian flow behavior of medium and highly concentrated solutions of polyamidoamine (PAMAM) dendrimers in ethylenediamine (EDA) solvent. *Macromolecules* **1998**, *31*, 4498−4510.
(38) Djeda, R.; Ruiz, J.; Astruc, D.; Satapathy, R.; Dash, B. P.; Hosmane, N. S. "Click" synthesis and properties of carborane-appended large dendrimers. *Inorg. Chem.* **2010**, *49*, 10702−10709.
(39) Wang, Y.; Grayson, S. M. Approaches for the preparation of non-linear amphiphilic polymers and their applications to drug delivery. *Adv. Drug Delivery Rev.* **2012**, *64*, 852−865.
(40) Milner, S. T.; Witten, T. A.; Cates, M. E. Theory of the grafted polymer brush. *Macromolecules* **1988**, *21*, 2610−2619.
(41) Murat, M.; Grest, G. S. Interaction between grafted polymeric brushes—a molecular-dynamics study. *Phys. Rev. Lett.* **1989**, *63*, 1074−1077.
(42) Murat, M.; Grest, G. S. Structure of a grafted polymer brush—a molecular-dynamics simulation. *Macromolecules* **1989**, *22*, 4054−4059.
(43) Chen, C. Y.; Tang, P.; Qiu, F.; Shi, A. C. Excluded volume effects in compressed polymer brushes: a density functional theory. *J. Chem. Phys.* **2015**, *142*, 124904.
(44) Francis, R.; Taton, D.; Logan, J. L.; Masse, P.; Gnanou, Y.; Duran, R. S. Synthesis and surface properties of amphiphilic star-shaped and dendrimer-like copolymers based on polystyrene core and poly(ethylene oxide) corona. *Macromolecules* **2003**, *36*, 8253−8259.
(45) Giupponi, G.; Buzza, D. M. A. A Monte Carlo study of amphiphilic dendrimers: spontaneous asymmetry and dendron separation. *J. Chem. Phys.* **2005**, *122*, 194903.
(46) Markelov, D. A.; Landeranta, E.; Gotlib, Y. Y. Influence of modified terminal segments on dynamic modulus and viscosity of dendrimer. *Macromol. Theory Simul.* **2010**, *19*, 158−169.
(47) Osawa, K.; Imae, T.; Ujihara, M.; Harada, A.; Ochi, K.; Ishihara, K.; Yusa, S. Preparation of amphiphilic diblock copolymers with pendant hydrophilic phosphorylcholine and hydrophobic dendron groups and their self-association behavior in water. *J. Polym. Sci., Part A: Polym. Chem.* **2013**, *51*, 4923−4931.
(48) Markelov, D. A.; Polotsky, A. A.; Birshtein, T. M. Formation of a "hollow" interior in the fourth-generation dendrimer with attached oligomeric terminal segments. *J. Phys. Chem. B* **2014**, *118*, 14961−14971.
(49) Xu, Y.; Chen, X.; Han, X.; Xu, S.; Liu, H.; Hu, Y. Lock/unlock mechanism of solvent-responsive binary polymer brushes: density functional theory approach. *Langmuir* **2013**, *29*, 4988−4997.
(50) Yu, Y.-X.; Wu, J. Density functional theory for inhomogeneous mixtures of polymeric fluids. *J. Chem. Phys.* **2002**, *117*, 2368−2376.
(51) Cao, D. P.; Wu, J. Z. Surface-induced phase transitions in ultrathin films of block copolymers. *J. Chem. Phys.* **2005**, *122*, 194703.
(52) Xu, X.; Cao, D. Density functional theory for adsorption of colloids on the polymer-tethered surfaces: effect of polymer chain architecture. *J. Chem. Phys.* **2009**, *130*, 164901.
(53) Meng, D.; Hjelm, R. P.; Hu, J. M.; Wu, J. Z. A theoretical model for the dynamic structure of hepatitis B nucleocapsid. *Biophys. J.* **2011**, *101*, 2476−2484.
(54) Rosenfeld, Y. Free-energy model for the inhomogeneous hard-sphere fluid mixture and density-functional theory of freezing. *Phys. Rev. Lett.* **1989**, *63*, 980−983.
(55) Wertheim, M. S. Thermodynamic perturbation-theory of polymerization. *J. Chem. Phys.* **1987**, *87*, 7323−7331.
(56) Cheng, L. S.; Cao, D. P. A hybrid approach for microscopic properties and self-assembly of dendrimers between two hard walls. *J. Phys. Chem. B* **2007**, *111*, 10775−10784.
(57) Xu, X.; Cao, D.; Zhang, X.; Wang, W. Universal version of density-functional theory for polymers with complex architecture. *Phys. Rev. E* **2009**, *79*, 021805.
(58) Stechemesser, S.; Eimer, W. Solvent-dependent swelling of poly(amido amine) starburst dendrimers. *Macromolecules* **1997**, *30*, 2204−2206.
(59) De Backer, S.; Prinzie, Y.; Verheijen, W.; Smet, M.; Desmedt, K.; Dehaen, W.; De Schryver, F. C. Solvent dependence of the


DOI: 10.1021/acs.jpcb.6b03005
*J. Phys. Chem. B* 2016, 120, 5553−5563

hydrodynamical volume of dendrimers with a rubicene core. *J. Phys. Chem. A* **1998**, *102*, 5451−5455.
(60) Topp, A.; Bauer, B. J.; Klimash, J. W.; Spindler, R.; Tomalia, D. A.; Amis, E. J. Probing the location of the terminal groups of dendrimers in dilute solution. *Macromolecules* **1999**, *32*, 7226−7231.
(61) Natali, S.; Mijovic, J. Molecular dynamics of PEG-dendrimer blends and PEGylated dendrimers. *Macromolecules* **2009**, *42*, 6799−6807.
(62) Amirova, A. I.; Belyaeva, E. V.; Tarabukina, E. B.; Sheremet'eva, N. A.; Muzafarov, A. M.; Filippov, A. P. Effect of fluorinated substituents on hydrodynamic and conformational properties of hyperbranched polycarbosilane in solutions. *Polym. Sci., Ser. C* **2010**, *52*, 70−78.
(63) Markelov, D. A.; Matveev, V. V.; Ingman, P.; Nikolaeva, M. N.; Lahderanta, E.; Shevelev, V. A.; Boiko, N. I. NMR studies of carbosilane dendrimer with terminal mesogenic groups. *J. Phys. Chem. B* **2010**, *114*, 4159−4165.
(64) Aumanen, J.; Teobaldi, G.; Zerbetto, F.; Korppi-Tommola, J. The effect of temperature on the internal dynamics of dansylated POPAM dendrimers. *RSC Adv.* **2011**, *1*, 1778−1787.
(65) Leibler, L. Theory of Microphase Separation in Block Co-Polymers. *Macromolecules* **1980**, *13*, 1602−1617.



DOI: 10.1021/acs.jpcb.6b03005
*J. Phys. Chem. B* 2016, 120, 5553−5563